Title
Conformational equilibria of light-activated rhodopsin in nanodiscs

Journal
Proceedings of the National Academy of Sciences of the United States of America, 114(16)

ISSN
0027-8424

Authors
Van Eps, Ned
Caro, Lydia N
Morizumi, Takefumi
et al.

Publication Date
2017-04-18

DOI
10.1073/pnas.1620405114

Peer reviewed

Conformational equilibria of light-activated rhodopsin in nanodiscs

Ned Van Eps[a,b,1], Lydia N. Caro[c,2], Takefumi Morizumi[c], Ana Karin Kusnetzow[a,b,3], Michal Szczepek[d], Klaus Peter Hofmann[d], Timothy H. Bayburt[e], Stephen G. Sligar[e], Oliver P. Ernst[c,f,4], and Wayne L. Hubbell[a,b,4]

[a]Department of Chemistry and Biochemistry, University of California, Los Angeles, CA 90095; [b]Jules Stein Eye Institute, University of California, Los Angeles, CA 90095; [c]Department of Biochemistry, University of Toronto, Toronto, ON, Canada M5S 1A8; [d]Institut für Medizinische Physik und Biophysik, Charité–Universitätsmedizin Berlin, 10117 Berlin, Germany; [e]Department of Biochemistry, University of Illinois at Urbana–Champaign, Champaign, IL 61801; and [f]Department of Molecular Genetics, University of Toronto, Toronto, ON, Canada M5S 1A8

Contributed by Wayne L. Hubbell, December 16, 2016 (sent for review October 14, 2016; reviewed by David L. Farrens and Heinz-Juergen Steinhoff)

Conformational equilibria of G-protein–coupled receptors (GPCRs) are intimately involved in intracellular signaling. Here conformational substates of the GPCR rhodopsin are investigated in micelles of dodecyl maltoside (DDM) and in phospholipid nanodiscs by monitoring the spatial positions of transmembrane helices 6 and 7 at the cytoplasmic surface using site-directed spin labeling and double electron–electron resonance spectroscopy. The photoactivated receptor in DDM is dominated by one conformation with weak pH dependence. In nanodiscs, however, an ensemble of pH-dependent conformational substates is observed, even at pH 6.0 where the MIIbH$^+$ form defined by proton uptake and optical spectroscopic methods is reported to be the sole species present in native disk membranes. In nanodiscs, the ensemble of substates in the photoactivated receptor spontaneously decays to that characteristic of the inactive state with a lifetime of ∼16 min at 20 °C. Importantly, transducin binding to the activated receptor selects a subset of the ensemble in which multiple substates are apparently retained. The results indicate that in a native-like lipid environment rhodopsin activation is not analogous to a simple binary switch between two defined conformations, but the activated receptor is in equilibrium between multiple conformers that in principle could recognize different binding partners.

rhodopsin | GPCR | conformational heterogeneity | nanodiscs | double electron–electron resonance

G-protein–coupled receptors (GPCRs) are central components of protein–protein interaction networks and can serve as hubs that link the extracellular environment of cells to intracellular signaling events (1). As such, they interact with several intracellular proteins (i.e., arrestins, G proteins, kinases). To obtain such diversity in molecular interaction, GPCRs are thought to be in equilibrium between multiple conformations at the cytoplasmic surface (2–4), enabling conformation-dependent interactions with different partners.

The rod photoreceptor rhodopsin has served as a model for members in the class A family of GPCRs. In native membranes (5–7) and reconstituted liposomes (8, 9), photoactivated rhodopsin within milliseconds reaches a pH-dependent quasi-equilibrium between states designated MI and MII, which are distinguished by their optical absorbance maxima and signature absorbances in the infrared (10–12). The optically identified MII state has been found to consist of isochromic substates, namely MIIa, MIIb, and MIIbH$^+$ (13–15) (Fig. 1*A*). MIIbH$^+$, populated at pH 6.0, is thought to be the functionally active substate that recognizes the cognate G-protein transducin (8, 15, 16).

Early data relating global protein structural changes to activation in a GPCR were provided by continuous wave (CW) site-directed spin labeling (SDSL)-Electron Paramagnetic Resonance (EPR) studies in rhodopsin, where it was shown that a generally outward motion of TM6 and a smaller inward motion of TM7 at the cytoplasmic surface were hallmarks of activation in dodecyl maltoside (DDM) micelles (17, 18). High-resolution distance mapping with SDSL and double electron–electron resonance (DEER) in DDM micelles revealed the directions and magnitudes of the motions (19), and the structural changes were subsequently confirmed by crystal structures of the inactive and active states (20, 21). At the cytoplasmic surface, crystal structures (21), solid-state NMR (22), SDSL (17), and infrared spectroscopy (23) found additional movements involving TM5. In the SDSL–EPR studies, TM5 motion was detected at site 231 in the aqueous extension of TM5, but not at site 225 in the bilayer domain (17); this is a site used in the present studies. Collectively, the data from SDSL–EPR in DDM and crystal structures give the impression that rhodopsin is unique among GPCRs, acting essentially as a binary switch, moving from a unique inactive conformation to one representing the activated state. This would be in contrast to other GPCRs, which apparently have a complex conformational landscape even in detergent solutions (2, 24). One goal of this study is to directly examine the conformational repertoire of rhodopsin in native-like lipid bilayers using SDSL–EPR spectroscopy.

Previous CW SDSL–EPR studies with single spin labels indicated that the signature TM6 movement was retained in

Significance

The existence of multiple conformational substates of G-protein–coupled receptors in equilibrium may provide for the interaction with multiple partners at the same interface. Here we provide evidence that photoactivated rhodopsin exists in a manifold of conformational substates in a lipid environment, but not in the extensively studied dodecyl maltoside detergent micelles. Moreover, the photoactivated state decays spontaneously to the inactive state on a timescale of minutes. Remarkably, binding of the activated receptor to the cognate G protein strongly biases the receptor to an interacting state that retains more than one conformation, suggesting flexibility in the complex.

Author contributions: N.V.E., A.K.K., K.P.H., S.G.S., O.P.E., and W.L.H. designed research; N.V.E., L.N.C., T.M., A.K.K., and T.H.B. performed research; M.S. and T.H.B. contributed new reagents/analytic tools; N.V.E., O.P.E., and W.L.H. analyzed data; and N.V.E. and W.L.H. wrote the paper.

Reviewers: D.L.F., Oregon Health & Science University; and H.-J.S., University of Osnabrueck.

The authors declare no conflict of interest.

Freely available online through the PNAS open access option.

[1]Present address: Department of Biochemistry, University of Toronto, Toronto, ON, Canada M5S 1A8.

[2]Present address: Biotechnologie et Signalisation Cellulaire, UMR 7242 CNRS, Université de Strasbourg, 67412 Illkirch, France.

[3]Present address: Crinetics Pharmaceuticals Inc., San Diego, CA 92121.

[4]To whom correspondence may be addressed. Email: oliver.ernst@utoronto.ca or hubbellw@jsei.ucla.edu.

This article contains supporting information online at www.pnas.org/lookup/suppl/doi:10.1073/pnas.1620405114/-/DCSupplemental.

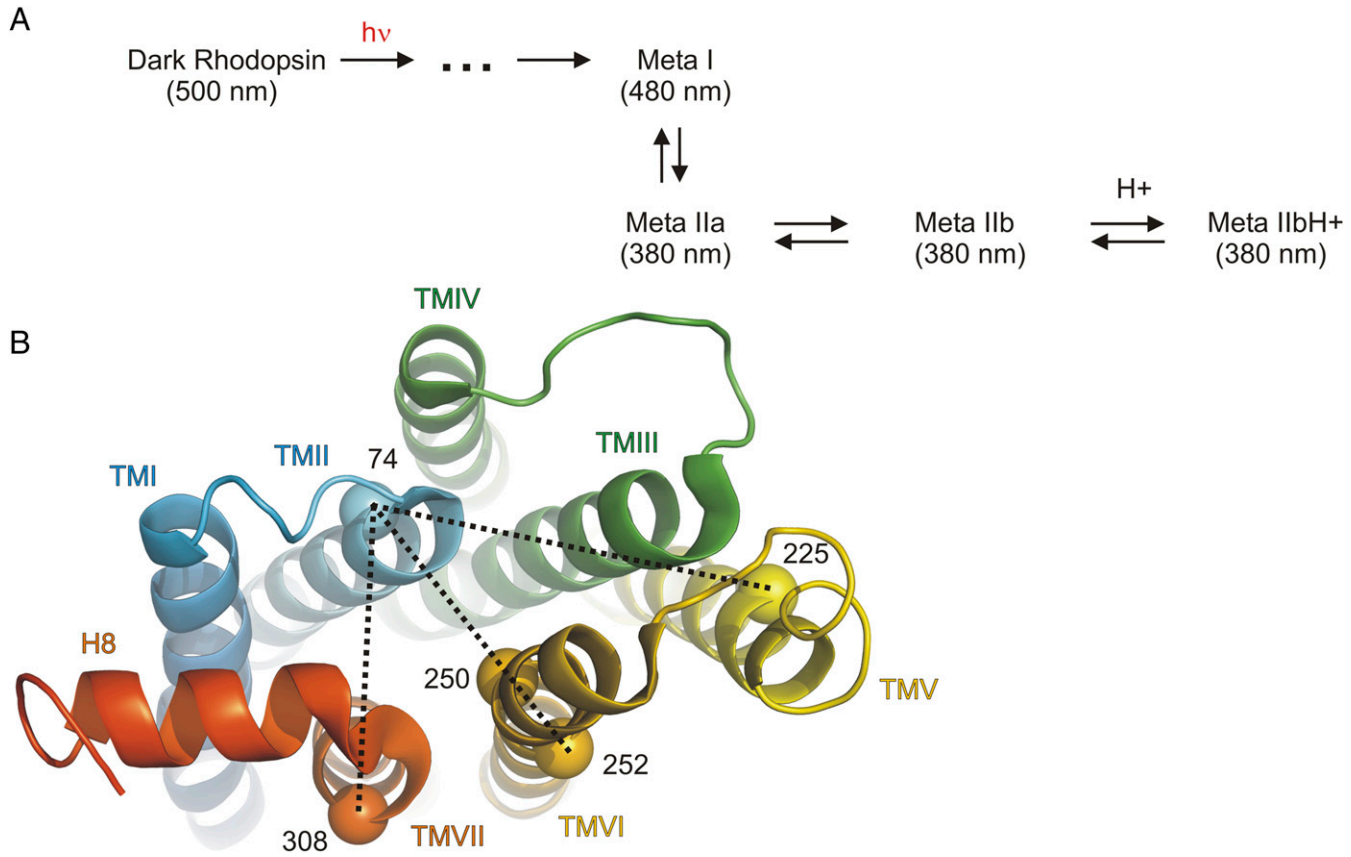

Fig. 1. Photo intermediates of rhodopsin and sites where nitroxide side chains (R1) were introduced. (*A*) Intermediates of rhodopsin defined by UV-vis and Fourier transform infrared spectroscopy (8, 16). As indicated, the MII state is known to be degenerate with three isochromic states. (*B*) Alpha carbon spheres on inactive rhodopsin (PDB ID 1GZM) identify sites were nitroxide side chains were introduced.

liposomes, and EPR spectral lineshape analysis suggested the presence of alternative conformations of the receptor in both the inactive and activated state in lipid bilayers, with shifts in populations upon activation (25). Although these studies indicated a greater complexity in the rhodopsin energy landscape than that inferred from crystal structures of the receptor, EPR spectral lineshapes give only a qualitative picture of conformational changes. For example, the lineshapes can be degenerate with respect to the number of states present, and, most importantly, contain no information on the magnitude of structural changes that correspond to the detected conformations.

In the present study, high-resolution SDSL–DEER distance mapping using pairs of spin labels is used to monitor the positions of TM5, TM6, and TM7 of rhodopsin in DDM and in phospholipid nanodiscs in which the receptor has properties similar to those in native membranes (26, 27). Distance mapping with DEER overcomes the limitations in CW lineshape analysis and provides a length scale to the energy landscape. Spin label sites to monitor the helix positions are located on the outer surface of the helices to avoid structural perturbations and are the same sites used in the earlier DEER distance mapping of rhodopsin in DDM solutions (19). The behavior of activated rhodopsin in a lipid bilayer environment is of primary interest here, but a comparison with DDM provides a perspective on the influence of the lipid environment. The DEER data obtained here for rhodopsin in DDM are in excellent agreement with the study of Altenbach et al. (19), but recent advances in instrumentation (28) (Q band vs. X band) and data analysis (29) permit increased resolution of details in the distance distributions.

In DDM the photoactivated receptor appears to be in a dominant single conformation with positions of TM5, TM6, and TM7 in good agreement with crystal structures of the activated state. However, in nanodiscs multiple discrete components are resolved, and the relative populations are strongly pH-dependent, indicating that the conformations are in equilibrium. In DDM, the distance distributions are only weakly dependent on pH. Remarkably, in nanodiscs but not DDM, the manifold of conformations in the activated state spontaneously relaxes on a minute timescale to the conformation characteristic of the inactive receptor. In the inactive receptor in both DDM and nanodiscs, dominant populations of TM6 and TM7 are at positions consistent with crystal structures of the inactive state, but also visit positions of low probability similar to those in the activated receptor structure.

The cytoplasmic ends of helices TM6 and TM7 are apparently involved in the recognition of the G protein, arrestin, and kinase (30–32), and the conformational heterogeneity in these regions of the activated receptor in nanodiscs may be involved in selective recognition of these or other binding partners. Indeed, the binding of a G protein is shown to select a particular receptor structure that itself has multiple conformations, suggesting flexibility in the complex.

Results

In the background of the rhodopsin C140S/C316S mutant, in which surface-exposed reactive cysteine residues were replaced by nonreactive serine residues, the R1 nitroxide side chain was introduced pairwise using SDSL methods (33) to monitor the intramolecular distances between a reference site at residue 74 in

TM2 to sites 225, 252, and 308 in TM5, TM6, and TM7, respectively (Fig. 1*B*), using DEER spectroscopy. Site 74C in TM2 was used as a reference site due to its discrete spatial localization observed in previous SDSL studies (19) and the static nature of TM2 inferred from crystallographic studies (20, 21). In one case, a single R1 residue was introduced at site 250 in TM6 to monitor the kinetics of motion of TM6 using CW SDSL–EPR methods (Fig. 1*B*).

Spin-labeled rhodopsin mutant pairs containing R1 were incorporated into MSP1E3D1 nanodiscs that contain 70% 1-palmitoyl-2-oleoyl-*sn*-glycero-3-phosphocholine (POPC) and 30% 1-palmitoyl-2-oleoyl-*sn*-glycero-3-phospho-L-serine (POPS) for spectroscopic studies using published procedures (34). CW–EPR spectra of the double mutants show only subtle lineshape changes upon light activation (Fig. S1), indicating that the environment of the label is largely unchanged upon activation. Titrations (pH) of spin-labeled and WT-activated rhodopsin in nanodiscs show a similar ratio of the optically defined metarhodopsin photo-intermediates MI and MII that are observed for native membranes (5) (Fig. S2).

In this article, the term "inactive" will refer to rhodopsin with 11-*cis* retinal inverse agonist bound (the "dark" state), and "activated rhodopsin" will refer to any form containing the agonist all-*trans*-retinal. As shown in Fig. 1, the activated form is degenerate, consisting of MI, MIIa, MIIb, and MIIbH$^+$ the populations of which depend on pH in a membrane environment. As mentioned above, MIIbH$^+$ is thought to be the functionally active form with respect to transducin activation.

The Inactive State and MIIbH$^+$ Are Not Single Conformations. Fig. 2*A* shows the DEER distance distributions that monitor the positions of TM5, TM6, and TM7 at pH 6.0 in DDM and nanodiscs for the inactive state (gray) and immediately after photoactivation (30 s) (red). The primary DEER data and fits to obtain the distance distributions are given in Figs. S3 and S4. Fig. 2*B* shows the corresponding UV-visible absorption spectra that document the nearly quantitative conversion of the inactive state (500 nm absorbance) to the MII species (380 nm). In DDM and in native disk membranes at pH 6.0, the functionally active MIIbH$^+$ species is essentially quantitatively populated (8, 35, 36).

In the inactive state the distributions for TM5, TM6, and TM7 in both DDM and nanodiscs have the most probable distances in good agreement with predictions based on modeling R1 in a crystal structure of the inactive receptor (PDB ID 1GZM; 30, 29, and 29 Å, respectively) (Fig. S5). However, the distributions are not monomodal, but have satellite components of lower population that appear as shoulders on the main peak (dashed lines, Fig. 2*A*). This is particularly evident in the distribution for TM6. The significance of these satellite peaks will be discussed below. Overall, the distance distributions are relatively similar in DDM and nanodiscs in the inactive receptor, but the satellite populations are suppressed in nanodiscs relative to DDM.

In the photoactivated receptor, dramatic differences between the conformations in DDM and nanodiscs become apparent. The smallest difference is for TM5, where after photoactivation in DDM the distance distribution shifts to a longer distance by ~1 Å to a position corresponding to the shoulder in the distribution of the inactive state. This small change reproduces that previously reported and emphasizes the reproducibility and high resolution of the DEER distance mapping. In nanodiscs, the change due to activation is absent. Thus, in nanodiscs, both TM2 and TM5 at the level of sites 74 and 225, respectively, do

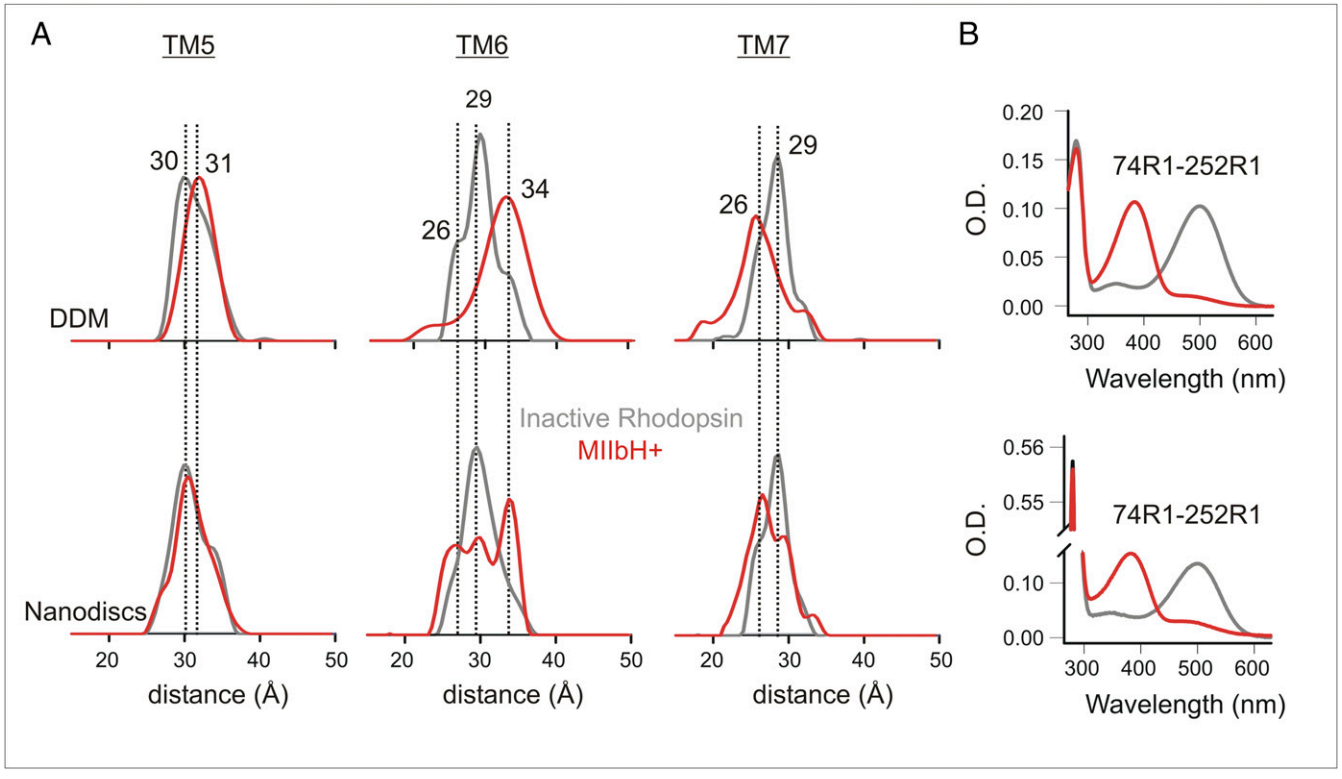

Fig. 2. Comparison of DEER distance distributions and UV-visible spectra for the rhodopsin mutants in DDM versus nanodiscs. (*A*) Normalized DEER distance distributions for pairs of R1 residues that monitor the positions of TM5, TM6, and TM7 for the inactive and active states in DDM and nanodiscs. The distances of prominent features in the distributions are identified. (*B*) UV-visible spectra of the 74R1-252R1 double mutant in DDM and nanodiscs; other pairs gave similar results. All data were acquired at pH 6.0. The large absorbance at 280 nm in nanodiscs arises from absorbance of the scaffold protein surrounding the nanodisc.

not move upon activation. The very small change in DDM could be due either to a small movement of 74R1 or 225R1 or both.

For TM6 in DDM, activation results in a shift in the population by 5 Å to a longer distance, as previously observed, resulting in a dominant (>90%) relatively broad population centered at 34 Å. This position is in good agreement with modeling of R1 in a crystal structure of activated rhodopsin (21) (PDB ID 3PXO; Fig. S5). Interestingly, this position corresponds to one of the minor components in the inactive state distribution. The situation in nanodiscs is strikingly different. At pH 6.0, where $MIIbH^+$ is reported to be the dominant population in a membrane environment (8, 35, 36), the distance distribution for TM6 has three resolved components of comparable populations at positions corresponding to the populations in the inactive state in both DDM and nanodiscs. The populations at 29 Å and 34 Å apparently correspond to the inactive and active state crystal structures. The shorter distance at 26 Å can be accounted for by a clockwise rotation of TM6 as viewed from the cytoplasmic surface (*Discussion*).

For TM7, the distribution for the inactive receptor in both DDM and nanodiscs is very similar, with a main peak at 29 Å and a poorly resolved shoulder at ~ 26 Å. Upon activation in DDM, the most probable population shifts by ~ 2–3 Å inward, in good agreement with earlier work (19) and with comparisons of R1 modeled in crystal structures of the inactive and active receptors (Fig. S5). This new position appears to correspond to the shoulder in the inactive state. The situation is similar in nanodiscs, except that a resolved population exists at the position of the inactive receptor.

The Conformational Substates of Activated Rhodopsin in Nanodiscs Are in a pH-Dependent Equilibrium. It is clear from the above results that the optically defined MI and MII intermediates cannot be correlated with a particular protein conformation. Nevertheless, the populations of the DEER detected conformations in nanodiscs in the activated receptor shift with pH, as do the relative populations of the MI and MII states detected optically. Fig. 3*A* shows the pH dependence of distance distributions in DDM and nanodiscs that monitor the positions of helices TM5, TM6, and TM7 relative to site 74 in TM2 in the activated receptor; for reference, there are essentially no changes with pH in the inactive receptor, and the distributions are as in Fig. 2. Fig. 3*B* shows the pH dependence in the UV-Vis absorbance spectra for double-labeled mutant 74R1/252R1; the data for the other pairs are identical. The pH 6.0 DEER data for TM6 is reproduced from Fig. 2 for comparison.

As the pH is changed in the range from 6.0 to 8.0, there are only small changes in the distance distributions in DDM. However, in nanodiscs there are clear shifts in the relative populations of resolved components in the distributions for TM6 and TM7, indicating that these populations are in equilibrium; there are no changes in the distribution monitoring TM5. The general shifts in population are toward the active conformational state as the pH becomes more acidic, as expected (11). At pH 8.0 where the MI population is ~60% (Fig. S2), the distributions of TM6 and TM7 approach those of the inactive state, generally consistent with an electron crystallography structure of MI that shows no changes in the position of the helices relative to the inactive state (37).

The Activated Conformational Manifold of Rhodopsin in Nanodiscs Spontaneously Decays to the Inactive State. In native membranes near neutral pH and room temperature, the ability of activated rhodopsin to induce nucleotide exchange in transducin spontaneously decays on the timescale of minutes (38), corresponding to the decay of the MI/MII photoproduct equilibrium directly or via an intermediate designated MIII to opsin and all-*trans* retinal (39). To explore the correlation of the functional decay with

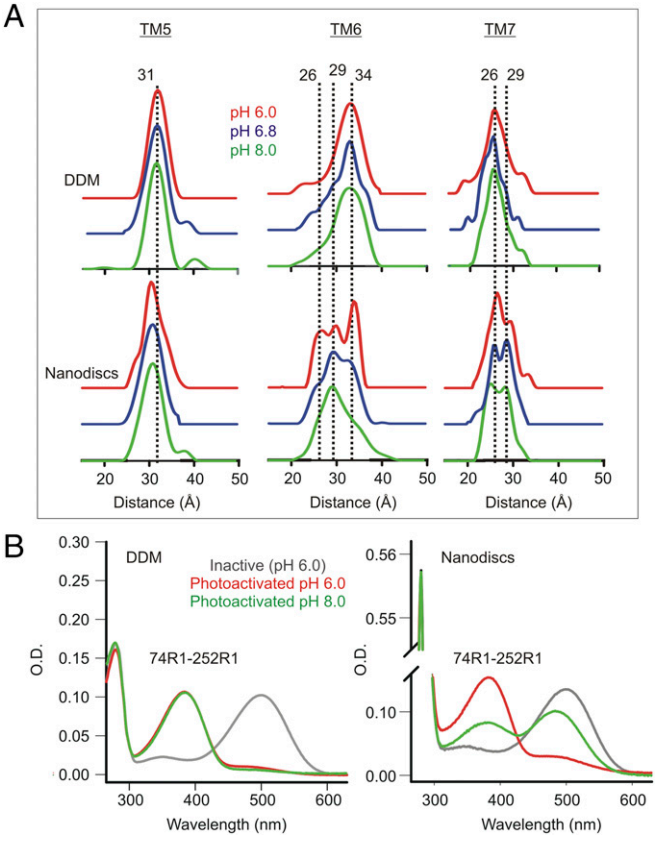

Fig. 3. pH dependence of DEER distance distributions and UV-visible spectra for activated rhodopsin in DDM or nanodiscs. (*A*) DEER distance distributions for pairs that monitor the position of TM5, TM6, and TM7. (*B*) UV-visible spectra of the 74R1-252R1 double mutant; other spin-labeled pairs and wild-type rhodopsin (Fig. S2) gave similar results.

global structural changes in the receptor, the distance distributions at pH 6.8 were determined immediately following activation (~30 s) and after 3 h postactivation. Remarkably, a spontaneous and complete reversal of TM6 displacement was observed for the activated receptor in nanodiscs (Fig. 4*A*). Spontaneous reversibility was also investigated for the TM6 at pH 6.0, where the largest changes occur with activation. For nanodiscs, reversibility is complete within 30 min following light activation (Fig. 4*B*), a time in which both opsin and MIII coexist (40) (Fig. S6), indicating that MIII has a configuration similar to the dark state and opsin with respect to TM6. In DDM solutions, spontaneous reversal of TM6 does not occur, but the distance distribution simply broadens over time, suggesting increased flexibility of the protein (Fig. 4*B*).

To measure the time constant for the spontaneous decay, time-resolved CW-EPR measurements were made that monitored lineshape changes for the single mutant 250R1. Site 250 is on the inner surface of TM6 (Fig. 1*B*), and nitroxide labels at this position are immobilized by tertiary contacts with the protein in the inactive state where TM6 is in the inward-most location (black trace, Fig. 4*C*). Upon outward motion of TM6 that accompanies activation, constraints on the motion of R1 are removed, and the spectral intensity changes in regions that reflect increased mobility (17, 25) (arrow, red trace, Fig. 4*C*). Upon structural relaxation, the spectral change quantitatively reverses. The kinetics of the structural relaxation was monitored by intensity changes in the EPR signal at a single field position (arrow in Fig. 4*C*). The rise time of the signal was fit with a single exponential function with a lifetime of 16 ± 3 min. This

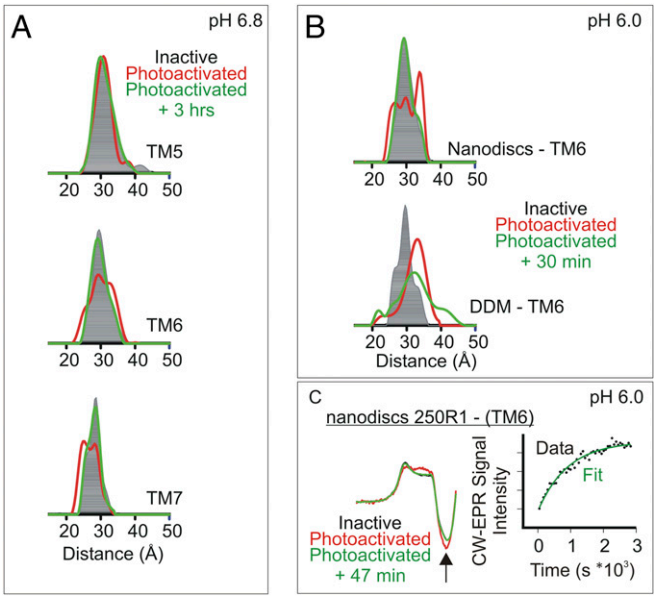

Fig. 4. Decay of the rhodopsin active state in nanodiscs. (*A*) Distance distributions monitoring the positions of TM5, TM6, and TM7 at pH 6.8 in the inactive state (gray), 30 s after photoactivation (red) and 3 h postactivation (green). (*B*) Distance distributions monitoring the position of TM6 at pH 6.0 for rhodopsin in nanodiscs (*Upper*) and DDM (*Lower*). Distributions shown are for the inactive state (gray), 30 s after photoactivation (red) and 30 min postactivation, where structural relaxation is apparently complete in the nanodisc. (*C*) Kinetics of the structural reversal of TM6 monitored by the CW-EPR spectra of 250R1 (see *Results*). The EPR signal intensity was measured as a function of time after activation at the field position indicated (arrow). The low field line of the EPR spectrum is shown for clarity. Single exponential fits to the data yielded a lifetime of 16 ± 3 min at 20 °C.

rate correlates well with MIII and opsin formation observed in native membranes (40).

G-Protein Binding to the Activated Receptor in Nanodiscs Selects a Subset of the Conformational Space. Activated rhodopsin binds its cognate G protein, transducin, to form a stable complex in membranes in the absence of GTP (41). For rhodopsin in nanodiscs, complex formation is complete with a twofold excess of transducin in the absence of GTP (42). When transducin is added in 2.5-fold excess to activated rhodopsin in nanodiscs at pH 6.8, a dramatic shift in the populations of conformers toward the fully outward and inward positions of TM6 and TM7, respectively, occurs (Fig. 5, *Upper*). The resulting distributions closely resemble those of fully active rhodopsin in DDM (Fig. 5, *Lower*). For TM6, there is no resolved population corresponding to the inactive structure (29 Å), consistent with complete formation of the complex, but remarkably a small population of the short distance (26 Å) persists. For TM7, both the active (26 Å) and inactive (29 Å) states are present, although the active state is the majority. No structural change is observed when transducin is added to the inactive receptor.

Discussion

Rhodopsin in Nanodiscs: The Activated State. Hallmarks of rhodopsin activation as defined by SDSL–EPR studies are an outward rigid body motion of TM6 and an inward displacement of the cytoplasmic termination of TM7 with only small motions of TM5 monitored at site 225 (17, 19). Although crystal structures of active and inactive rhodopsin indicate substantial motions of TM5, these changes occur in the cytoplasmic extensions of the helix in the aqueous phase, but not at site 225, consistent with the SDSL–EPR data (Fig. S5). The above features appear to be characteristic of the rhodopsin family of GPCRs based on the available crystal structures (43). Not seen in the crystal structure of active rhodopsin is that, in a native-like phospholipid environment at low pH where MIIbH$^+$ is strongly enriched, the fully activated receptor is apparently in equilibrium between multiple conformations of comparable populations defined by the positions of TM6 and TM7 at the cytoplasmic surface.

For TM6 in the activated receptor, two of the three states observed correspond to helix positions in the inactive and active crystal structures (Fig. S5 and Fig. 6). The third conformation, identified by the short distance at 26 Å, can be accounted for by a clockwise rotation of TM6 by about 40° when it is in the outward position. Such a rotation was suggested earlier to explain CW–EPR distance mapping in activated rhodopsin (44), and a smaller rotation in this sense is in fact present in the crystal structure of activated rhodopsin (21). It could be argued that the short distance arises from the appearance of a new R1 rotamer of 252R1 caused by a local structure change. However, the invariance of the CW lineshape upon activation (17) (Fig. S1) argues against this interpretation because the motion of the nitroxide and hence the lineshape is exquisitely sensitive to the local environment, which would be changed in a new rotamer state. One reasonable interpretation of the data is that the three states of TM6 are (*i*) in the inactive position (TM6°); (*ii*) tilted outward by 5–6 Å (TM6*); and (*iii*) tilted outward and rotated clockwise (TM6**). For TM7, two states are clearly resolved, each corresponding to positions of TM7 resolved in the inactive and active crystal structures; these are designated TM7° and TM7*.

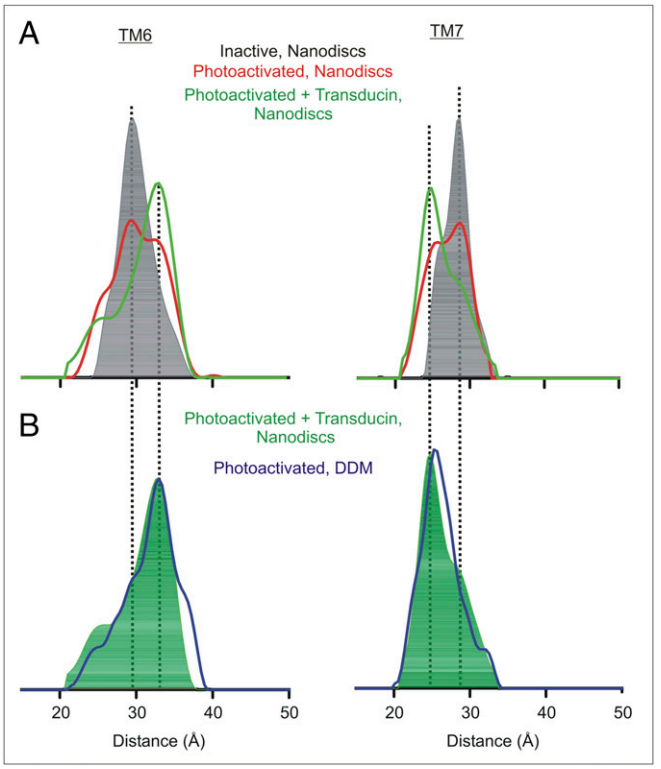

Fig. 5. Conformational selection by transducin at pH 6.8. (*A*) DEER distance distributions for R1 pairs monitoring the positions of TM6 and TM7 in the inactive state (gray), photoactivated (red line), and in the presence of 2.5× excess of transducin (green line). (*B*) Comparing distance distributions of the transducin-bound state in nanodiscs from the *A* graph (solid green line) with the active state in DDM (solid blue line in the *B* graph). Primary DEER data are provided in Fig. S7.

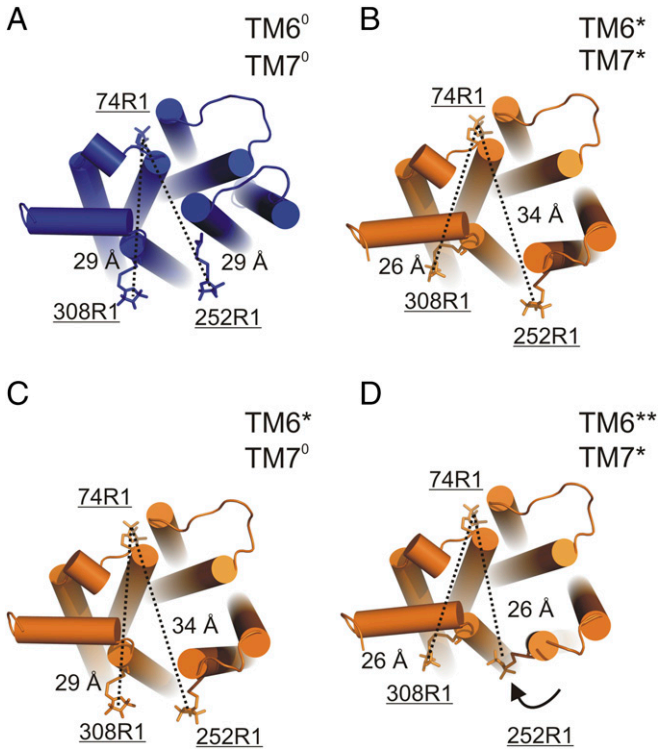

Fig. 6. Four possible substates of rhodopsin suggested by the DEER distance distributions and modeling. (*A*) The inactive state (TM6°, TM7°). (*B*) TM6 tilted outward and TM7 inward (TM6*, TM7*). (*C*) A state with TM6 tilted outward (TM6*, TM7°). (*D*) A state with TM6 tilted outward and rotated and TM7 moved inward (TM6**, TM7*). The models in *A* and *B* were obtained by modeling the R1 side chain in the crystal structures of the inactive (1GZM) and activated (3PXO) crystal structures, respectively. Models for the noncrystallographically observed states of *C* and *D* were obtained by tilting TM6 in *A* and rotating TM6 in *B*, respectively. In each model, the dashed line is the interspin distance between nitroxides of R1, which was modeled using known rotamers of R1 (Fig. S5). Data analysis suggests that the G protein selects TM6* and TM7* as dominant populations.

From the data presented here, it cannot be determined whether or not the distinct TM6 and TM7 states occur independently or are correlated. However, modeling based on crystal structures suggests that an inward motion of TM7 cannot occur without the outward displacement of TM6 to avoid steric clashes in the packed interior of the protein. Moreover, the rotation of TM6* to form TM6** may require the inward position of TM7 (TM7*); otherwise, residue 252R1 in TM6 would have steric clashes with residues in TM7 and become immobilized, which is not observed. In the context of this model, there would be minimally four conformational states of the receptor, namely {TM6°, TM7°}, {TM6*, TM7°}, {TM6*, TM7*}, and {TM6**, TM7*}. Fig. 6 shows schematic representations of these speculative conformations. The considerations above argue for an appearance of the conformations in a time-ordered fashion (16). The {TM6**, TM7*} conformation has not been observed previously by optical spectroscopy, and it remains to be determined how it relates to the equilibrium of MII substates.

Which of the conformations represents the fully activated receptor with respect to G-protein recognition? An answer is provided by the distance distributions with transducin bound (Fig. 5). The G protein apparently selects predominantly the state designated {TM6*, TM7*}. However, within the context of the models presented in Fig. 6, there must also be smaller populations of {TM6**, TM7*} and {TM6*, TM7°} present to account for the other distances observed, suggesting the surprising result that the helices remain in exchange between more than one state even in the G-protein–bound state. The formation of the complex is apparently complete in the nanodisc, based on the reduction of the major population at the distance corresponding to the inactive state. In addition, earlier studies of transducin binding to activated rhodopsin in nanodiscs showed that complex formation is complete under the conditions used here (42). Thus, it is tentatively concluded that the presence of multiple populations in the complex is not due to incomplete complex formation but rather to flexibility of the structure within the complex itself.

Rhodopsin in Nanodiscs: The Inactive State. Interestingly, even with the 11-*cis* retinal inverse agonist bound in the inactive receptor, three populations of TM6 and two of TM7 are detected at the same distances found in the active state, although those corresponding to TM6*, TM6**, and TM7* are strongly suppressed and are revealed only as shoulders in the distance distribution. The apo protein opsin is formed upon retinal dissociation, and the active structure relaxes spontaneously to one essentially identical to the inactive state with respect to the distances mapped. Nevertheless, neither the inactive receptor nor opsin activate transducin, indicating that additional requirements must be met for recognition of the G protein. Such a requirement could be for a coordinated fluctuation of the helices with a lifetime sufficiently long to form a collision complex or, alternatively, the release of additional constraints on the structure due to retinal isomerization. The pH independence of the populations in the inactive state favors the latter interpretation. Earlier studies reported by Kim et al. found that certain mutations could displace the cytoplasmic regions of the helices without activation of the G protein (45). Collectively, these results suggest a weak coupling of the ligand-binding site with the cytoplasmic surface of the receptor. A model consistent with the data is that the cytoplasmic terminations of the helices in the inactive state are flexible and can visit alternative conformations similar to those in the activated state, but additional changes due to agonist binding are required for a productive complex. At least one of the additional changes must be in the region of Glu134, the protonation site leading to the formation of MIIbH$^+$. This follows from the pH independence of the conformations in the inactive state.

In the β_2 adrenergic receptor and the adenosine A_{2A} receptor, multiple conformations were found in both the unliganded protein and with an inverse agonist bound, also suggesting a weak coupling of the cytoplasmic surface with the ligand-binding site (2, 24).

Rhodopsin in DDM. Remarkably, distances corresponding to the three states of TM6 and two of TM7 are also observed in the inactive receptor in DDM. This situation cannot be accounted for by some fraction of inadvertently activated receptor because in DDM the activated state does not reveal the three populations (Fig. 2). Moreover, the spectral ratio A280/A500 ~ 1.6 for the purified receptor in DDM solution is characteristic of pure inactive rhodopsin (46).

In the activated state with the all-*trans* retinal agonist bound, there is a dominant state with a most probable distance corresponding to the fully activated state observed in the corresponding crystal structure, but the distribution is relatively broad. On the timescale where the structure spontaneously decays to the inactive state in nanodiscs, little change in the most probable position of TM6 occurs, but the distribution becomes increasingly broad, indicating an increased conformational heterogeneity, possibly due to local unfolding.

The unique behavior of activated rhodopsin in DDM relative to bilayers may be related to binding of detergent monomers to protein surface sites or cavities to stabilize a particular conformation, but apparently not to the retinal binding site (47). An

alternative (but not mutually exclusive) thermodynamic model posits that the conformations of the protein may be determined by an interfacial tension between the protein and detergent or lipid environment (48). If a detergent or lipid interacts more strongly with itself than with the protein, the interfacial tension is positive, leading to a compressive force on the protein. On the other hand, a more favorable interaction with the protein than with itself leads to a negative tension and an expansion of the protein interfacial area. In the context of this simple model, the shift in TM6 toward the inward position in bilayers relative to DDM would be interpreted as a positive interfacial tension in the bilayer, whereas the strong bias to the outward position in DDM would arise from a negative tension. The compressive/expansive forces can be large (48).

Summary. The key results presented here are the following: (*i*) in DDM micelles, the activated receptor is essentially a single conformation, as previously reported, corresponding to a fully activated MIIbH$^+$ state; (*ii*) in nanodiscs, activated rhodopsin exists in a pH-dependent conformational equilibrium between substates of comparable amounts. Two of the conformations correspond to the inactive and active crystal structures of the receptor, and the third may involve an additional rotation of TM6; (*iii*) in both DDM and nanodiscs, the inactive receptor visits active-like conformations with low probability, but additional structural or dynamic requirements must be met for formation of a productive complex; (*iv*) upon formation of a complex with the G protein in nanodiscs, the position of the conformational equilibrium is strongly shifted to a new state that appears to retain multiple conformations, suggesting flexibility in the complex.

The multiple states of activated rhodopsin in nanodiscs may be involved in the recognition of multiple binding partners, and this will be the subject of a future study.

Materials and Methods

Protein Expression and Spin Labeling of Rhodopsin Mutants. An expression construct containing the base mutant (C140S/C316S) was used to create four different DNA plasmid constructs (250C, 74C/252C, 74C/225C, and 74C/308C) via the QuikChange site-directed mutagenesis method (Agilent Technologies). Expression and purification of the retinal regenerated rhodopsin and derivatization with spin labels (1-oxyl-2,2,5,5-tetramethyl-Δ3-pyrroline-3-methyl methanethiosulfonate) was done as described (25). The spin-labeled mutants were eluted from a 1D4 antibody resin in either 90 mM *n*-octyl-β-D-glucopyranoside (OG) (for incorporation into nanodiscs) or DDM detergent using a peptide with sequence identity to the last nine amino acids of rhodopsin's C terminus (American Peptide).

Expression and Purification of Nanodisc Scaffold Proteins. A pET-28a vector containing the MSP1E3D1 gene construct (49) was transformed into *Escherichia coli* BL21Gold(DE3) cells for growth and expression. The DNA plasmid was obtained from addgene (https://www.addgene.org/), which had been deposited in their repository by Stephen G. Sligar, University of Illinois at Urbana–Champaign. *E. coli* cell cultures were induced with 1 mM isopropyl β-D-1-thiogalactopyranoside overnight at room temperature. The cells were harvested by centrifugation at 8,000 × *g* for 10 min and stored at −20 °C until purification.

The *E. coli* cell pellets were resuspended in lysis buffer (20 mM sodium phosphate, 1% Triton X-100, 1 mM phenylmethylsulfonyl fluoride, pH 7.4) and sonicated, and the cell lysate was cleared by centrifugation at 43,146 × *g* for 30 min in a SS-34 Sorval rotor. The cleared lysate was loaded onto a nickel NTA column, and the column was washed sequentially with the following buffers: (*i*) 40 mM Tris, 0.3 M NaCl, 1% Triton, pH 8.0; (*ii*) 40 mM Tris, 0.3 M NaCl, 50 mM cholate, 20 mM imidazole, pH 8.0; and (*iii*) 40 mM Tris, 0.3 M NaCl, 50 mM imidazole, pH 8.0. Finally, the MSP1E3D1 scaffold protein was eluted from the resin with 40 mM Tris, 0.3 M NaCl, 0.5 M imidazole, pH 8.0, and dialyzed overnight against buffer A (20 mM Tris, 0.1 M NaCl, 0.5 mM EDTA, pH 7.4) at 4 °C.

Purification of Wild-Type Rhodopsin and Transducin from Bovine Retinas. Rod cell disk membranes were purified from bovine retinas as previously described (50). The native membrane samples were solubilized in the presence of 90 mM OG at 4 °C for 4 h. The lysate was cleared by centrifugation at 43,146 × *g* for 30 min in a SS-34 Sorval rotor. The cleared lysate was loaded onto a 1D4 antibody resin for purification and eluted in a buffer containing 90 mM OG using the rhodopsin C-terminal peptide. Transducin was purified from native disk membranes using established protocols (51).

Construction of Rhodopsin Nanodiscs. Nanodiscs containing mutant or wild-type rhodopsin were made as previously described (34). The phospholipid composition of the discs was 70% POPC and 30% POPS. For some receptor characterizations, rhodopsin-containing nanodiscs were purified away from the empty discs. This was done by passing the nanodiscs over a rhodopsin 1D4 antibody resin. The resulting nanodisc preparation lacked empty nanodiscs or spurious liposomes. Purity of the receptor containing nanodisc samples was judged by the ratio of absorbance between 280 nm and 500 nm.

UV-Visible Spectroscopy. UV-visible spectroscopy of rhodopsin in nanodiscs was performed using a Cary 50 spectrophotometer with Peltier assembly. MI, MII, and dark rhodopsin basis spectra were acquired as described (25). For fits to the rhodopsin nanodisc samples, the wavelength region of 350–650 nm was used to avoid absorption from the nanodisc scaffold protein. Linear regression fits were generated in Excel to estimate the fraction of MII within the nanodisc samples, and scatter plots of the fraction of MII versus pH were fit using Henderson Hasselbach equations in Matlab (Fig. S2).

Rhodopsin active-state decay was followed in nanodiscs at pH 6.0 (Fig. S6) by collecting UV-visible spectra every 2 min following photobleaching. Single-wavelength data at 475 nm are plotted as a function of time and fit to a single exponential rise.

Fluorescence Spectroscopy. Decay of photoactivated rhodopsin in nanodiscs was measured by monitoring tryptophan fluorescence changes at pH 6.0 as previously described (52). A Cary Eclipse fluorescence spectrometer with Peltier assembly was used with excitation and emission wavelengths of 290 nm and 330 nm, respectively (Fig. S6). Fluorescence data were fit to a single exponential function in Matlab.

DEER and CW–EPR. For DEER measurements, spin-labeled rhodopsin samples (generally 30–100 μM) in buffer containing 20% (vol/vol) glycerol were flash-frozen within quartz capillaries (1.5 mm i.d. and 1.8 mm o.d.). After freezing, they were loaded into an EN 5107D2 resonator, and Q-band measurements were performed at 80,000 on a Bruker Elexsys 580 spectrometer with a Super Q-FTu Bridge. For the four-pulse DEER experiment used here, a 32-ns π-pump pulse was applied to the low field peak of the nitroxide field-swept spectrum, and the observer π/2 (16 ns) and π (32 ns) pulses were positioned 50 MHz (17.8 G) upfield, which corresponds to the nitroxide center line. Distance distributions were obtained from the raw dipolar evolution data using the LabVIEW (National Instruments) program "LongDistances" [developed by Christian Altenbach, University of California, Los Angeles (UCLA)] that can be downloaded from biochemistry.ucla.edu/biochem/Faculty/Hubbell/. Documentation in the program describes the methods and practical details for background determination and distance distributions. A few of the DEER experiments were performed using a Q-band Bruker Elexsys 580 instrument located at the University of Toronto. Reproducibility of the raw data was excellent from sample to sample and independent of instruments (UCLA and University of Toronto). The raw, background uncorrected data are provided in Figs. S8 and S9. It has been shown that a variation in the second echo period of the four-pulse DEER experiment can lead to shifts in the distance of a given population for the same sample. In the present experiments, the variation of the second echo period was no more than 1.4 μs, which would not significantly influence the reported distributions (53).

CW-EPR measurements were performed on either a Bruker Elexsys 580 spectrometer (UCLA) or a Varian E-109 spectrometer (UCLA). Spectra were acquired over a 100-G range at room temperature at X-band microwave frequencies. Field-modulation amplitudes were 2 G. The data were typically averages of 20–40 scans.

Experiments in the presence of transducin were performed using a 2.5-fold molar excess of the G protein relative to rhodopsin. The G protein was washed using Amicon concentrators to remove excess GDP before addition to the rhodopsin nanodiscs.

ACKNOWLEDGMENTS. We thank Christian Altenbach and Matthias Elgeti for their critical reading of the manuscript. This work was supported by NIH Grant R01EY05216 (to W.L.H.); the Canada Excellence Research Chair program (O.P.E.); the Anne and Max Tanenbaum Chair in Neuroscience (O.P.E.); the Jules Stein Professor Endowment (W.L.H.); the National Eye Institute Core Grant P30EY00331 and NIH Grant GM R35118145 (to S.G.S.); and a European Research Council advanced grant (to K.P.H.).

1. Kobilka BK, Deupi X (2007) Conformational complexity of G-protein-coupled receptors. *Trends Pharmacol Sci* 28(8):397–406.
2. Manglik A, et al. (2015) Structural insights into the dynamic process of β2-adrenergic receptor signaling. *Cell* 161(5):1101–1111.
3. Nygaard R, et al. (2013) The dynamic process of β(2)-adrenergic receptor activation. *Cell* 152(3):532–542.
4. Bock A, Kostenis E, Tränkle C, Lohse MJ, Mohr K (2014) Pilot the pulse: Controlling the multiplicity of receptor dynamics. *Trends Pharmacol Sci* 35(12):630–638.
5. Jäger S, Szundi I, Lewis JW, Mah TL, Kliger DS (1998) Effects of pH on rhodopsin photointermediates from lumirhodopsin to metarhodopsin II. *Biochemistry* 37(19): 6998–7005.
6. Lüdeke S, Lórenz Fonfría VA, Siebert F, Vogel R (2006) Time-resolved rapid-scan Fourier transform infrared difference spectroscopy on a noncyclic photosystem: Rhodopsin photointermediates from Lumi to Meta II. *Biopolymers* 83(2):159–169.
7. Szundi I, Epps J, Lewis JW, Kliger DS (2010) Temperature dependence of the lumirhodopsin I-lumirhodopsin II equilibrium. *Biochemistry* 49(28):5852–5858.
8. Mahalingam M, Martínez-Mayorga K, Brown MF, Vogel R (2008) Two protonation switches control rhodopsin activation in membranes. *Proc Natl Acad Sci USA* 105(46): 17795–17800.
9. Ye S, et al. (2010) Tracking G-protein-coupled receptor activation using genetically encoded infrared probes. *Nature* 464(7293):1386–1389.
10. Matthews RG, Hubbard R, Brown PK, Wald G (1963) Tautomeric forms of metarhodopsin. *J Gen Physiol* 47:215–240.
11. Vogel R, Siebert F (2003) Fourier transform IR spectroscopy study for new insights into molecular properties and activation mechanisms of visual pigment rhodopsin. *Biopolymers* 72(3):133–148.
12. Brown MF (2012) UV-visible and infrared methods for investigating lipid-rhodopsin membrane interactions. *Methods Mol Biol* 914:127–153.
13. Arnis S, Hofmann KP (1993) Two different forms of metarhodopsin II: Schiff base deprotonation precedes proton uptake and signaling state. *Proc Natl Acad Sci USA* 90(16):7849–7853.
14. Arnis S, Fahmy K, Hofmann KP, Sakmar TP (1994) A conserved carboxylic acid group mediates light-dependent proton uptake and signaling by rhodopsin. *J Biol Chem* 269(39):23879–23881.
15. Fahmy K, Sakmar TP (1993) Regulation of the rhodopsin-transducin interaction by a highly conserved carboxylic acid group. *Biochemistry* 32(28):7229–7236.
16. Knierim B, Hofmann KP, Ernst OP, Hubbell WL (2007) Sequence of late molecular events in the activation of rhodopsin. *Proc Natl Acad Sci USA* 104(51):20290–20295.
17. Altenbach C, et al. (1996) Structural features and light-dependent changes in the cytoplasmic interhelical E-F loop region of rhodopsin: A site-directed spin-labeling study. *Biochemistry* 35(38):12470–12478.
18. Altenbach C, Cai K, Khorana HG, Hubbell WL (1999) Structural features and light-dependent changes in the sequence 306-322 extending from helix VII to the palmitoylation sites in rhodopsin: A site-directed spin-labeling study. *Biochemistry* 38(25): 7931–7937.
19. Altenbach C, Kusnetzow AK, Ernst OP, Hofmann KP, Hubbell WL (2008) High-resolution distance mapping in rhodopsin reveals the pattern of helix movement due to activation. *Proc Natl Acad Sci USA* 105(21):7439–7444.
20. Zhou XE, Melcher K, Xu HE (2012) Structure and activation of rhodopsin. *Acta Pharmacol Sin* 33(3):291–299.
21. Choe HW, et al. (2011) Crystal structure of metarhodopsin II. *Nature* 471(7340): 651–655.
22. Ahuja S, et al. (2009) Helix movement is coupled to displacement of the second extracellular loop in rhodopsin activation. *Nat Struct Mol Biol* 16(2):168–175.
23. Elgeti M, et al. (2011) Conserved Tyr223(5.58) plays different roles in the activation and G-protein interaction of rhodopsin. *J Am Chem Soc* 133(18):7159–7165.
24. Ye L, Van Eps N, Zimmer M, Ernst OP, Prosser RS (2016) Activation of the A2A adenosine G-protein-coupled receptor by conformational selection. *Nature* 533(7602):265–268.
25. Kusnetzow AK, Altenbach C, Hubbell WL (2006) Conformational states and dynamics of rhodopsin in micelles and bilayers. *Biochemistry* 45(17):5538–5550.
26. Whorton MR, et al. (2008) Efficient coupling of transducin to monomeric rhodopsin in a phospholipid bilayer. *J Biol Chem* 283(7):4387–4394.
27. Tsukamoto H, Szundi I, Lewis JW, Farrens DL, Kliger DS (2011) Rhodopsin in nanodiscs has native membrane-like photointermediates. *Biochemistry* 50(22):5086–5091.
28. Ghimire H, McCarrick RM, Budil DE, Lorigan GA (2009) Significantly improved sensitivity of Q-band PELDOR/DEER experiments relative to X-band is observed in measuring the intercoil distance of a leucine zipper motif peptide (GCN4-LZ). *Biochemistry* 48(25):5782–5784.
29. Jeschke G (2012) DEER distance measurements on proteins. *Annu Rev Phys Chem* 63: 419–446.
30. Scheerer P, et al. (2008) Crystal structure of opsin in its G-protein-interacting conformation. *Nature* 455(7212):497–502.
31. Kang Y, et al. (2015) Crystal structure of rhodopsin bound to arrestin by femtosecond X-ray laser. *Nature* 523(7562):561–567.
32. Thurmond RL, Creuzenet C, Reeves PJ, Khorana HG (1997) Structure and function in rhodopsin: Peptide sequences in the cytoplasmic loops of rhodopsin are intimately involved in interaction with rhodopsin kinase. *Proc Natl Acad Sci USA* 94(5): 1715–1720.
33. Hubbell WL, López CJ, Altenbach C, Yang Z (2013) Technological advances in site-directed spin labeling of proteins. *Curr Opin Struct Biol* 23(5):725–733.
34. Bayburt TH, Leitz AJ, Xie G, Oprian DD, Sligar SG (2007) Transducin activation by nanoscale lipid bilayers containing one and two rhodopsins. *J Biol Chem* 282(20): 14875–14881.
35. Lüdeke S, Mahalingam M, Vogel R (2009) Rhodopsin activation switches in a native membrane environment. *Photochem Photobiol* 85(2):437–441.
36. Elgeti M, et al. (2013) Precision vs flexibility in GPCR signaling. *J Am Chem Soc* 135(33): 12305–12312.
37. Ruprecht JJ, Mielke T, Vogel R, Villa C, Schertler GF (2004) Electron crystallography reveals the structure of metarhodopsin I. *EMBO J* 23(18):3609–3620.
38. Bennett N, Michel-Villaz M, Kühn H (1982) Light-induced interaction between rhodopsin and the GTP-binding protein. Metarhodopsin II is the major photoproduct involved. *Eur J Biochem* 127(1):97–103.
39. Bartl FJ, Vogel R (2007) Structural and functional properties of metarhodopsin III: Recent spectroscopic studies on deactivation pathways of rhodopsin. *Phys Chem Chem Phys* 9(14):1648–1658.
40. Heck M, et al. (2003) Signaling states of rhodopsin. Formation of the storage form, metarhodopsin III, from active metarhodopsin II. *J Biol Chem* 278(5):3162–3169.
41. Kühn H, Bennett N, Michel-Villaz M, Chabre M (1981) Interactions between photoexcited rhodopsin and GTP-binding protein: Kinetic and stoichiometric analyses from light-scattering changes. *Proc Natl Acad Sci USA* 78(11):6873–6877.
42. D'Antona AM, Xie G, Sligar SG, Oprian DD (2014) Assembly of an activated rhodopsin-transducin complex in nanoscale lipid bilayers. *Biochemistry* 53(1):127–134.
43. Tehan BG, Bortolato A, Blaney FE, Weir MP, Mason JS (2014) Unifying family A GPCR theories of activation. *Pharmacol Ther* 143(1):51–60.
44. Farrens DL, Altenbach C, Yang K, Hubbell WL, Khorana HG (1996) Requirement of rigid-body motion of transmembrane helices for light activation of rhodopsin. *Science* 274(5288):768–770.
45. Kim JM, et al. (2004) Structural origins of constitutive activation in rhodopsin: Role of the K296/E113 salt bridge. *Proc Natl Acad Sci USA* 101(34):12508–12513.
46. Hong K, Knudsen PJ, Hubbell WL (1982) Purification of rhodopsin on hydroxyapatite columns, detergent exchange, and recombination with phospholipids. *Methods Enzymol* 81:144–150.
47. Park JH, et al. (2013) Opsin, a structural model for olfactory receptors? *Angew Chem Int Ed Engl* 52(42):11021–11024.
48. Baldwin PA, Hubbell WL (1985) Effects of lipid environment on the light-induced conformational changes of rhodopsin. 1. Absence of metarhodopsin II production in dimyristoylphosphatidylcholine recombinant membranes. *Biochemistry* 24(11): 2624–2632.
49. Denisov IG, Baas BJ, Grinkova YV, Sligar SG (2007) Cooperativity in cytochrome P450 3A4: Linkages in substrate binding, spin state, uncoupling, and product formation. *J Biol Chem* 282(10):7066–7076.
50. Van Eps N, et al. (2010) Electron paramagnetic resonance studies of functionally active, nitroxide spin-labeled peptide analogues of the C-terminus of a G-protein alpha subunit. *Biochemistry* 49(32):6877–6886.
51. Mazzoni MR, Malinski JA, Hamm HE (1991) Structural analysis of rod GTP-binding protein, Gt. Limited proteolytic digestion pattern of Gt with four proteases defines monoclonal antibody epitope. *J Biol Chem* 266(21):14072–14081.
52. Farrens DL, Khorana HG (1995) Structure and function in rhodopsin. Measurement of the rate of metarhodopsin II decay by fluorescence spectroscopy. *J Biol Chem* 270(10): 5073–5076.
53. Baber JL, Louis JM, Clore GM (2015) Dependence of distance distributions derived from double electron-electron resonance pulsed EPR spectroscopy on pulse-sequence time. *Angew Chem Int Ed Engl* 54(18):5336–5339.
54. Fleissner MR, Cascio D, Hubbell WL (2009) Structural origin of weakly ordered nitroxide motion in spin-labeled proteins. *Protein Sci* 18(5):893–908.